ENVIRONMENTAL STUDIES

Westerly induced precipitation increase drives near-surface ground ice gain on the Tibetan Plateau despite warming

Yi Zhao[1], Dongfeng Li[1,2]*, Jan Nitzbon[3], Zhuotong Nan[4], Yuqi Song[5], Xie Hu[5], Youhua Ran[6], Shang Tian[1], Rui Deng[1], Yingzhong Luo[1], Yiyi Li[1]

Near-surface ground ice loss is a key sign of permafrost degradation under global warming, dictating ground destabilization and carbon feedback. However, recent field evidence suggests that ground ice may locally accumulate, while the driving mechanisms remain unclear. Leveraging borehole ground ice observations, a physics-based permafrost model, and satellite-based ground deformation data, we identify an anomalous ice increase at the active layer bottom despite climate warming across the interior Tibetan Plateau, occupying 35% of plateau's permafrost area. Strengthened westerlies have enhanced precipitation, supplying additional soil moisture that refreezes at the active layer bottom and drives this unexpected ice gain. Freeze-thaw process associated with the accumulated ice amplifies ground deformation, destabilizing permafrost landscapes and threatening socioeconomic activities. This anomalous ice gain in permafrost regions, together with the Karakoram anomalous glacier mass increase, represents a divergent cryospheric ice gain against global ice loss under climate warming, highlighting that rapid precipitation increase may locally outweigh temperature in driving cryosphere evolution on the Tibetan Plateau.

INTRODUCTION

Permafrost, defined as ground remaining below 0°C for more than two consecutive years, encompasses approximately one-fifth of the Northern Hemisphere's land area and stores over 60% of the global soil carbon reservoir (*1*). Recent global warming has triggered widespread permafrost degradation across the world's cold regions (*2*, *3*). The Tibetan Plateau, which hosts the world's largest expanse of alpine permafrost, is highly sensitive and vulnerable to climate change (*4*). Over recent decades, the plateau has experienced marked climate warming (0.35°C/decade) at a rate of twice the global average (0.16°C/decade) (*5*), resulting in substantial permafrost degradation (*6*). This degradation has imposed considerable impacts on local landscape stability, ecosystem functioning, infrastructure safety, and greenhouse gas emissions (*7*–*9*), jeopardizing the sustainable development of over two billion people downstream.

Dynamics of near-surface ground ice, distributed at the active layer bottom and top of permafrost, represent a key indicator for evaluating permafrost degradation and assessing its environmental and socioeconomic impacts. With ongoing permafrost degradation, the pronounced variations of ice content within active layer and near-surface permafrost have been observed across global cold regions (*10*, *11*). The resulting landscape instability poses threats to human infrastructure in permafrost regions, leading to increased maintenance costs (*12*, *13*). Abrupt permafrost thaw triggered by the thaw of ground ice, such as thermokarst lakes and thaw slumps, can expose many meters of permafrost soil and greatly accelerate the release of the stored carbon, intensifying the permafrost-carbon feedback to climate warming (*14*–*16*). Moreover, on the Tibetan Plateau, thaw of near-surface ground ice serves as an important yet unsustainable source of water for many of Asia's major rivers and lakes (*17*–*19*). These additional water supplies transport large amounts of sediment and solutes from permafrost landscapes, with great impacts on regional aquatic ecosystems, hydropower facilities, and water resources security (*20*–*22*). Therefore, a holistic understanding of ground ice dynamics on the Tibetan Plateau is of great importance for the permafrost community and local policy-makers.

Despite the urgency, the response of near-surface ground ice to recent climate change across the Tibetan Plateau remains poorly understood. The primary challenge lies in the scarcity of large-scale, long-term observations. Ground ice data are typically derived from in-situ observations; however, the harsh environment and limited accessibility of the plateau severely limit the spatial and temporal coverage of boreholes (*23*, *24*). As an alternative, empirical parameterizations and physics-based models describing the relationship between near-surface ground ice and temperature have been used for large-scale investigation, demonstrating widespread ice loss across global permafrost regions (*25*–*27*). However, field experiments in Arctic permafrost regions have revealed that a contrasting ice accumulation may occur at the active layer bottom due to precipitation infiltration, despite local air temperature warming (*28*, *29*). Abnormal ground uplift has also been reported in the northwestern permafrost region of the Tibetan Plateau, potentially associated with precipitation-induced ground ice accumulation (*30*). This evidence may suggest a divergent yet underexplored regime of near-surface ice dynamics driven by precipitation in permafrost regions. Nevertheless, the underlying mechanisms driving this abnormal ice accumulation are still unclear.

Here, we propose a hypothesis that the rapid increase in precipitation may outweigh temperature as a dominant driver of near-surface

[1]Key Laboratory for Water and Sediment Sciences, Ministry of Education, College of Environmental Sciences and Engineering, Peking University, Beijing 100871, China. [2]State Key Laboratory of Plateau Ecology and Agriculture, Qinghai University, Xining 810016, China. [3]Permafrost Research Section, Alfred Wegener Institute Helmholtz Center for Polar and Marine Research, Telegrafenberg, Potsdam 14473, Germany. [4]State Key Laboratory of Climate System Prediction and Risk Management, Nanjing Normal University, Nanjing 210023, China. [5]College of Urban and Environmental Sciences, State Key Laboratory of Vegetation Structure, Function and Construction (VegLab), and Key Laboratory for Earth Surface Processes of the Ministry of Education, Peking University, Beijing 100871, China. [6]National Cryosphere Desert Data Center, State Key Laboratory of Cryospheric Science and Frozen Soil Engineering, Northwest Institute of Eco-Environment and Resources, Chinese Academy of Sciences, Lanzhou 730000, China.
*Corresponding author. Email: dongfeng.li@pku.edu.cn

ground ice dynamics. To test this hypothesis, we leverage extensive in situ borehole observations and a physics-based permafrost model to reconstruct 40-year (1979 to 2018) variations in near-surface ground ice across the Tibetan Plateau. We identify an anomalous ice increase trend at the active layer bottom under climate warming in the interior plateau, primarily driven by rising precipitation. This study offers a novel understanding of the near-surface ground ice dynamics in response to climate wetting, with crucial implications for adaptation and mitigation of permafrost evolution and its impacts on local infrastructure, ecosystems, and permafrost carbon feedback under a warming and wetting climate.

RESULTS

Anomalous ice gain at the active layer bottom

We compiled ground ice records from 369 boreholes across the permafrost regions of the Tibetan Plateau, including 194 drilled before 2000 and 175 drilled after 2000 (Fig. 1A and tables S1 and S2). At the regional scale, borehole records drilled after 2000 exhibit a markedly higher average volumetric ice content (0.25 m^3/m^3) than those drilled before 2000 (0.16 m^3/m^3) (Fig. 1B). The difference provides a first-order regional indication that ground ice has increased on the plateau after 2000, although the comparison may partly reflect climate and landscape heterogeneity among borehole sites (*31*). Meanwhile, the region has undergone permafrost degradation, evidenced by a relatively warm and fast-rising ground temperature (mean annual ground temperature exceeding −1.9°C and rising at a rate over 0.35°C/decade) (*5*). Ground ice in this region would theoretically be expected to decrease under climate warming, yet it has accumulated. This apparent anomalous ice gain under climate warming suggests a complex and previously underexplored response of permafrost to climate change, which we refer to here as permafrost anomaly.

We further select four pairs of spatially adjacent boreholes that include measurements both before and after 2000, reducing the influence of spatial heterogeneity of boreholes (Fig. 1C). Their close proximity (within ~2 km) and similar topography and climate allow a more controlled comparison of ground ice conditions. Across these paired sites, boreholes drilled after 2000 (0.21 m^3/m^3) generally show higher volumetric ice content than those before 2000 (0.13 m^3/m^3; Fig. 1C). Notably, the post-2000 ground ice increase exhibits pronounced heterogeneity in depth across all borehole pairs. The shallow active layer shows only a slight increase in ground ice, whereas the active layer bottom exhibits a substantial increase (Fig. 1C).

Using a physics-based permafrost modeling framework (fig. S1), we reconstruct the dynamics of frozen water content (FWC) at 0- to 3.2-m depth across the entire Tibetan Plateau from 1979 to 2018 and delineate the extent of this anomalous ice gain. Although simulated FWC represents only pore ice, its good agreement with borehole ground ice at depths of 0 to 3 m (fig. S3) and generally positive correlation with excess ice (*32*) suggest that it can serve as a reasonable proxy for near-surface ground ice. Accordingly, we identify that the anomalous ice gain is mainly distributed in the westerly influenced interior plateau, occupying 35% of the plateau's permafrost area (Fig. 1D). Ice gain regions associated with climate cooling, such as Pamir and parts of the Qilian Mountains, are not included in the anomalous regions (Fig. 1D, light green areas). Rising air temperatures have driven an overall soil temperature (ST) increase across the plateau (Fig. 2A and fig. S4, A and C). The southeastern monsoon–dominated plateau exhibits the expected decline in FWC (Fig. 1A). In contrast, the westerly controlled regions are largely characterized by a seemingly paradoxical increase in FWC (Fig. 1A and fig. S5, I and J) despite persistent warming (fig. S4C), reversing the plateau-wide FWC change trend to a net increase after 2000 (Figs. 1E and 2A). Notably, the simulations reproduce the pronounced post-2000 ice gain at the active layer bottom observed in borehole pairs. The magnitude and increase rate of FWC in the deep active layer (1.4 to 3.2 m) are substantially higher than those at shallower depths (Fig. 1E). The westerly controlled permafrost regions exhibit a net ground-ice increase of +144 km^3 within 0- to 3.2-m depth from 1979 to 2018, which offsets ice losses in the monsoon regions (−46.5 km^3) and results in an overall net ground-ice increase (+98 km^3) across the plateau's permafrost regions (fig. S6). The identified permafrost anomaly regions contribute a major fraction of this increase (+85 km^3; fig. S6).

FWC outputs from 10 models participating in the Coupled Model Intercomparison Project Phase 6 (CMIP6) are applied to examine whether large-scale climate simulations reproduce tendencies similar to the identified permafrost anomaly. Seven of the 10 models show increasing FWC accompanying air temperature warming in the interior plateau (fig. S7), in line with borehole observations and SHAW simulations, despite their coarse resolution and using different atmospheric and land-surface schemes. This multimodel agreement suggests that anomalous ground ice increase is unlikely to arise solely from biases in models and provides additional support for the existence of permafrost anomalies on the Tibetan Plateau from the modeling perspective.

Drivers of the permafrost anomaly

The occurrence of the anomalous ice gain at active layer bottom across the westerly influenced interior Tibetan Plateau is closely linked to increased precipitation. In general, variations in FWC are expected to be negatively correlated with air and ST. Consistent with this expectation, FWC declined in response to rising temperatures during the pre-2000 period (Figs. 1E and 2A). However, after 2000, the strengthening mid-latitude westerlies transport moisture from the Mediterranean-Iranian Plateau to the Tibetan Plateau (*4*, *33*), resulting in a rapid rise in precipitation across the interior plateau (Fig. 2A and fig. S4B). Correspondingly, the plateau-wide FWC trend turned from a pre-2000 decline to a post-2000 increase. Within the anomaly regions, FWC rising exhibits a strong positive correlation with precipitation increase (fig. S8B). Regions experiencing greater FWC gains correspond to more pronounced precipitation increases (Fig. 2B). In contrast, regions characterized by FWC declines are associated with decreasing or only marginally increasing precipitation and substantial climate warming (Fig. 2B).

By assessing precipitation changes and the associated dynamics of soil water content (SWC) and FWC before and after 2000, we elucidate a process-based mechanism by which precipitation drives FWC increase (Fig. 2, C to F). Mean annual precipitation has increased by 60% in the anomaly regions (227.5 ± 9.1 mm before 2000 versus 364.8 ± 12.1 mm after 2000). Rainfall contributes 87.3 mm of this increase, predominantly during the thaw season (Fig. 2C). Snowfall adds 49.9 mm, mainly between April and June but melts shortly thereafter (Fig. 2C), consistent with recent observations of increasing snowfall accompanied by shortening spring snow cover duration (*34*). The increased rainfall and snowmelt infiltrate into the thawed active layer (Fig. 2D), increasing SWC throughout the soil profile (Fig. 2E). These additional SWC subsequently refreeze during the freeze season, resulting in increased FWC after 2000 (Fig. 2F).

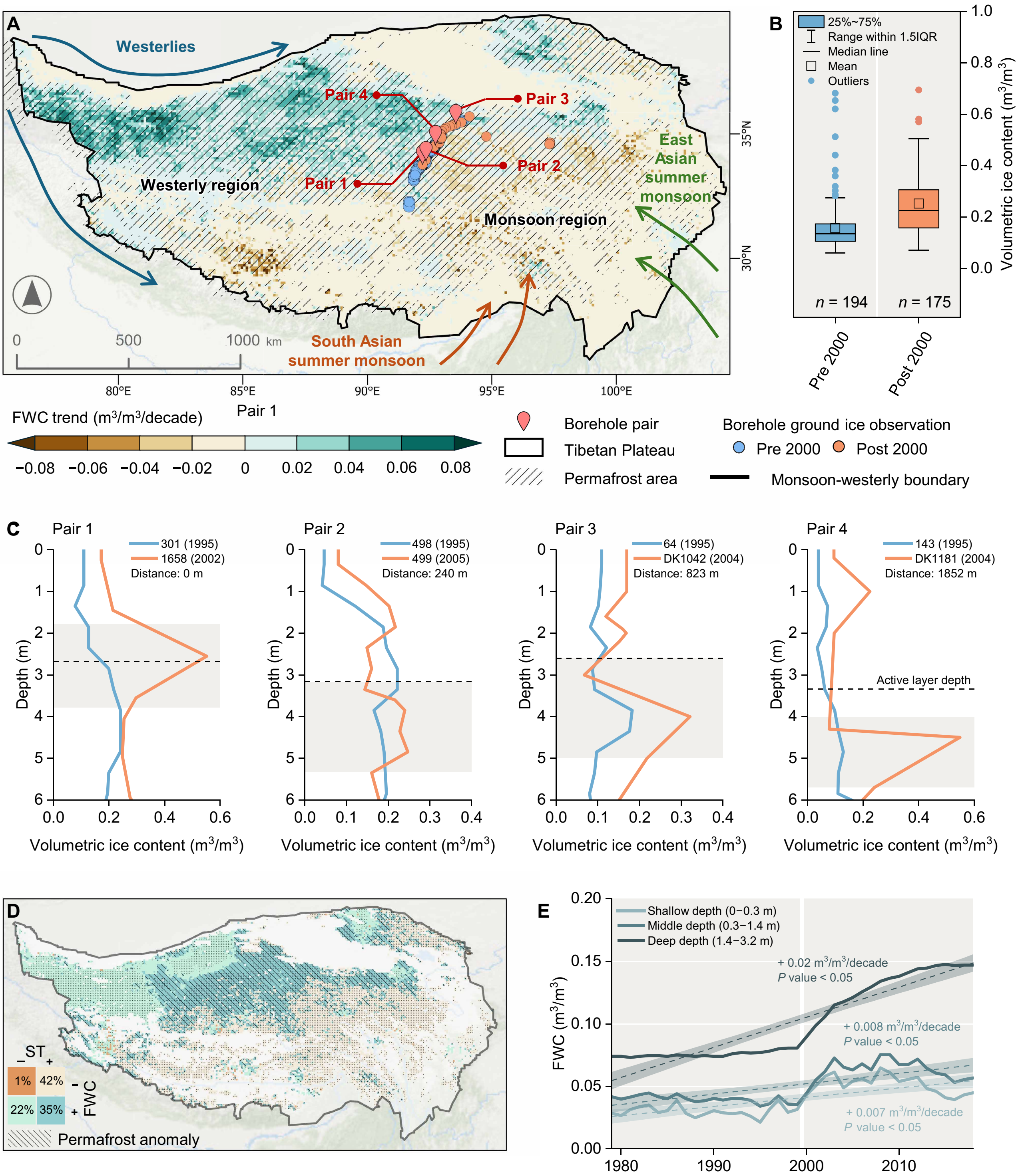

Fig. 1. Changes of near-surface ground ice on the Tibetan Plateau from 1979 to 2018. (**A**) The locations of boreholes (blue and yellow points) and representative borehole pairs (red marks), along with the simulated change trend of mean annual frozen water content (FWC) from 0- to 3.2-m depth by the SHAW model. The permafrost area distribution is provided by Obu (*1*). The boundary of the monsoon- and westerly controlled regions is provided by Wu *et al.* (*66*). (**B**) The volumetric ground ice content (m^3/m^3) measured by boreholes before and after 2000. (**C**) Vertical profiles of volumetric ground ice content from four spatially adjacent borehole pairs. Legends indicate the borehole IDs (see table S1) and drilling years. Dashed lines denote the depth of the active layer, and shading areas highlight depth intervals showing the most pronounced post-2000 ice increase for each pair. The locations of these borehole pairs are shown in (A). (**D**) Coupled dynamics of FWC and soil temperature (ST) across the permafrost regions of the Tibetan Plateau, classified into four regimes: ST decrease (−) & FWC−, ST− & FWC increase (+), ST+ & FWC−, and ST+ & FWC+. The permafrost anomaly corresponds to ST+ & FWC+ regime. Dots indicate grids with statistically significant trends ($P < 0.05$) in both ST and FWC. (**E**) The changes in simulated FWC at different depths within the permafrost anomaly regions. The dash lines denote the linear fitting curves and the shadings denote the 95% confidence intervals.

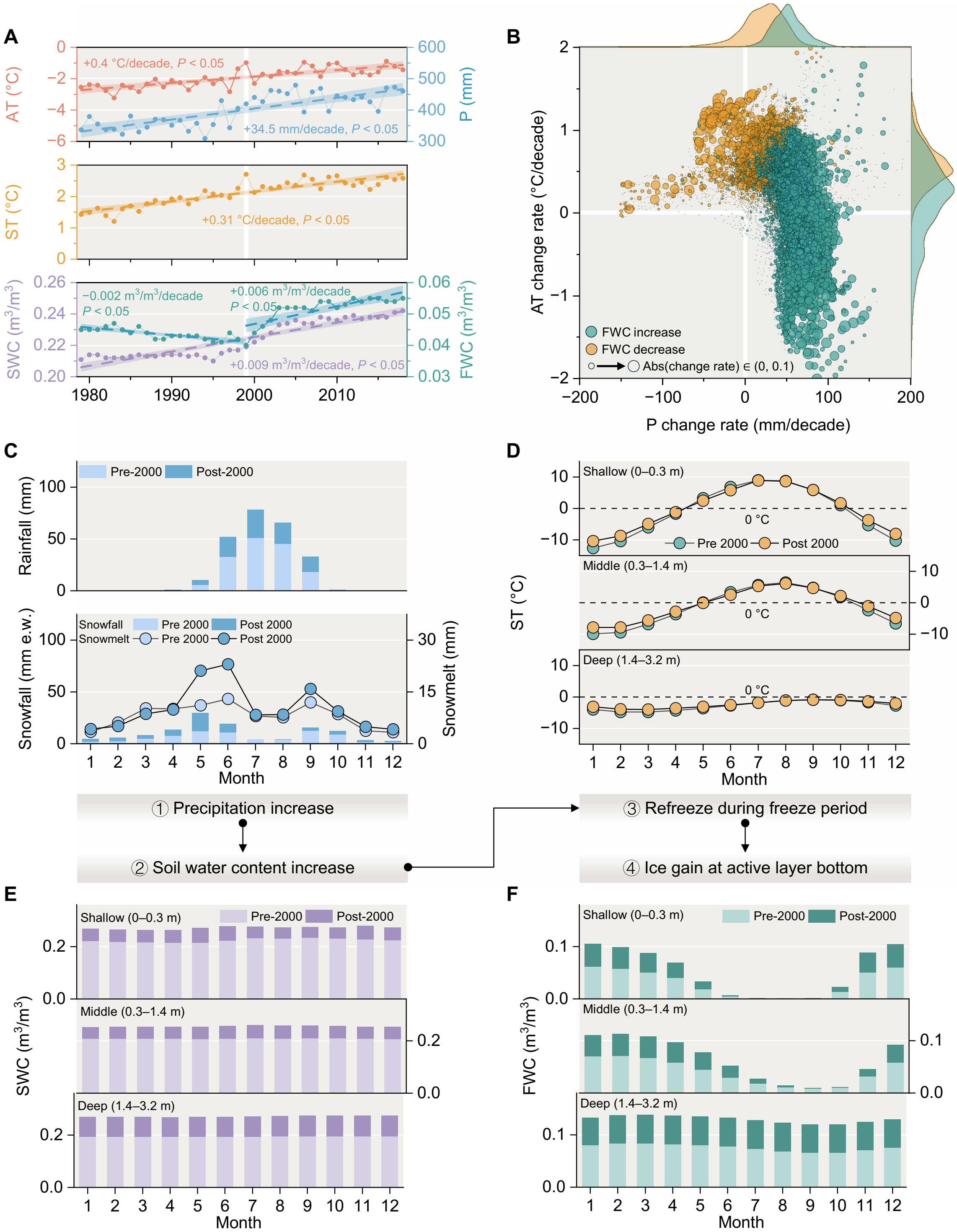

Fig. 2. Climatic controls on permafrost anomaly. (**A**) The time series of mean annual air temperature (AT), precipitation (P), simulated soil temperature (ST), soil water content (SWC), and frozen water content (FWC) from 0- to 3.2-m depth across the entire Tibetan Plateau from 1979 to 2018. The dash lines denote the linear fitting curves and the shadings denote the 95% confidence intervals. (**B**) The relationship between 40-year change rates of air temperature (AT), precipitation (P), and frozen water content (FWC, m^3/m^3/decade) for each 10-km grid on the Tibetan Plateau. Green circles indicate grids with increasing FWC, and yellow circles indicate grids with decreasing FWC. Circle size represents the absolute FWC change rate (m^3/m^3/decade), with larger circles indicating greater increases or decreases. The shading areas at the top and right sides denote the relative frequencies. (**C** to **F**) Process-based interpretation of the ice gain at active layer bottom in the anomaly regions, showing changes in monthly P (C), ST (D), SWC (E), and FWC (F) between the pre- and post-2000 periods within anomaly regions.

The deep active layer has a prolonged freezing period to refreeze infiltrated water and be retained as ice (Fig. 2D), thereby promoting year-round FWC accumulation (Fig. 2F) (*29*). In contrast, although FWC in the shallower layer (0 to 1.4 m) increases in the freezing season, it largely thaws during the thaw season (Fig. 2F), preventing long-term ice retention. Therefore, the anomalous ice accumulation is more likely to occur at the active layer bottom rather than at shallower depths (Fig. 1E).

Using the pre-2000 climate as a baseline, we conducted scenario experiments to disentangle the respective impacts of the rising precipitation and air temperature on FWC. When post-2000 precipitation was constrained to be at the pre-2000 levels (no wetting scenario), the FWC trends across most anomaly regions shifted from an upward trend (Fig. 1A) to a downward trend (Fig. 3, A and C), demonstrating the dominant role of post-2000 precipitation increase in driving the anomalous ice accumulation. Moreover, the rate of ST increase accelerated under this scenario (Fig. 3D), indicating that precipitation-induced FWC accumulation probably offset permafrost warming under climate warming, primarily owing to enhanced latent heat effects (*35*, *36*). This cooling effect of precipitation is consistent with recent observations across Northern Hemisphere permafrost regions (*37*). In contrast, when air temperature was held constant while precipitation increased after 2000 (no warming scenario), the persistently colder ST facilitates the refreezing efficiency of the additional SWC supplied by increased precipitation (Fig. 3, C and D), resulting in accelerated FWC accumulation (Fig. 3, B and C).

Moreover, topographic controls also contribute to the ice gain in the anomaly regions. Regions exhibiting the anomaly are typically characterized by high elevations (>4500 m) and gentle slopes (<10°) (fig. S9, A and C). Gentle slopes reduce downslope drainage and lateral runoff, facilitating the retention of additional soil moisture supplied by increasing precipitation. Meanwhile, high elevations provide sufficiently low temperatures to refreeze the supplied soil moisture from precipitation, leading to ice accumulation (fig. S9, B and D).

Linkages to permafrost landscape stability

The anomalous ice accumulation in the active layer bottom within permafrost regions is potentially linked to the intensified ground deformation. InSAR-derived surface deformation data indicate that anomaly regions exhibit greater seasonal ground deformation magnitude (18 ± 10 mm) in the vertical direction than other permafrost areas (14 ± 9 mm; Fig. 4, A and B). The accumulation and decay of ice within the active layer bottom enhance volumetric expansion and contraction associated with ice-water phase transitions during seasonal freeze-thaw cycles (*38*, *39*), thereby potentially amplifying seasonal frost heave and thaw subsidence in anomaly regions (*29*). Such enhanced seasonal deformation may weaken soil structure, increase surface erodibility, and destabilize near-surface permafrost landscapes (*29*, *40*). Consequently, anomalous ice accumulation may pose increasing risks to landscape stability and the long-term sustainability of ecosystems and infrastructure on permafrost terrain.

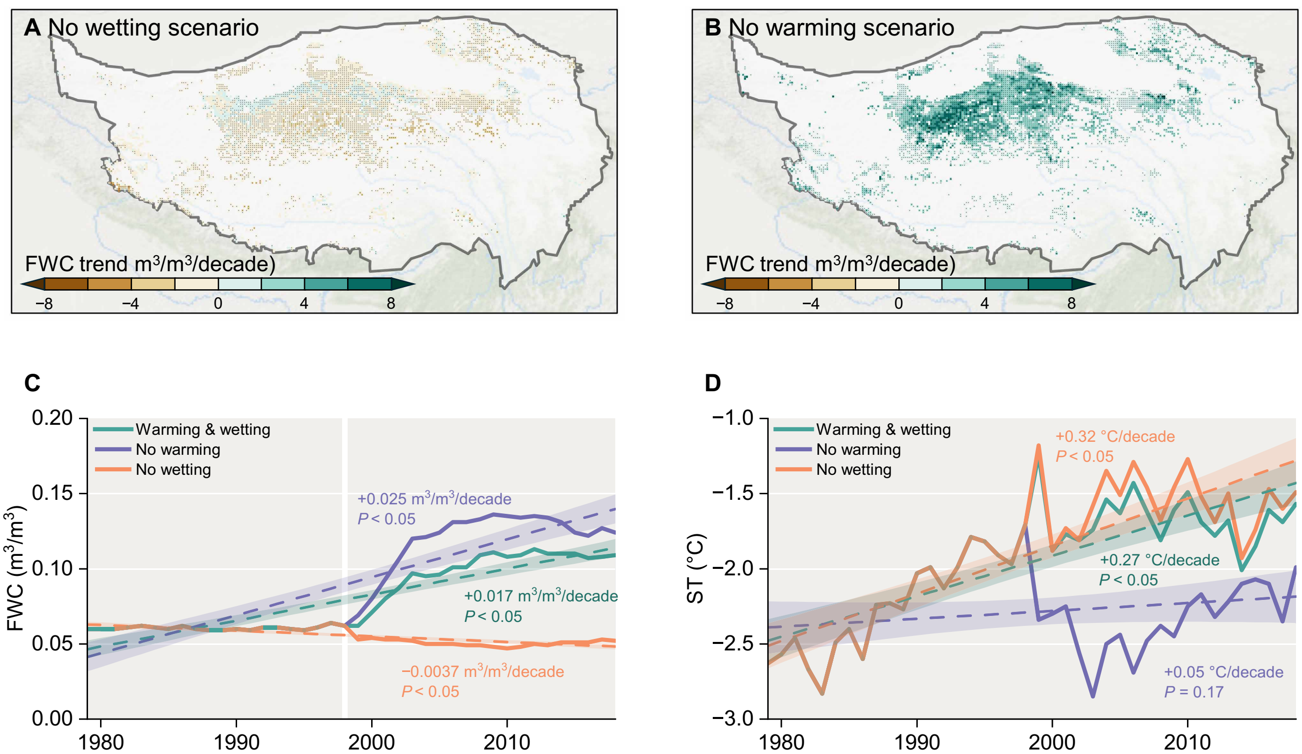

Fig. 3. Impacts of climate warming and wetting on anomalous ice gains. (**A** and **B**) Change trends of FWC in the anomaly regions from 1979 to 2018 under No wetting scenario and No warming scenario, respectively. Dots indicate grids with statistically significant trends ($P < 0.05$). (**C** and **D**) Changes of average FWC and ST in the anomaly regions from 1979 to 2018 under different scenarios. The dash lines denote the linear fitting curves, and the shadings denote the 95% confidence intervals. FWC presented here represents the mean annual values of the entire soil profile.

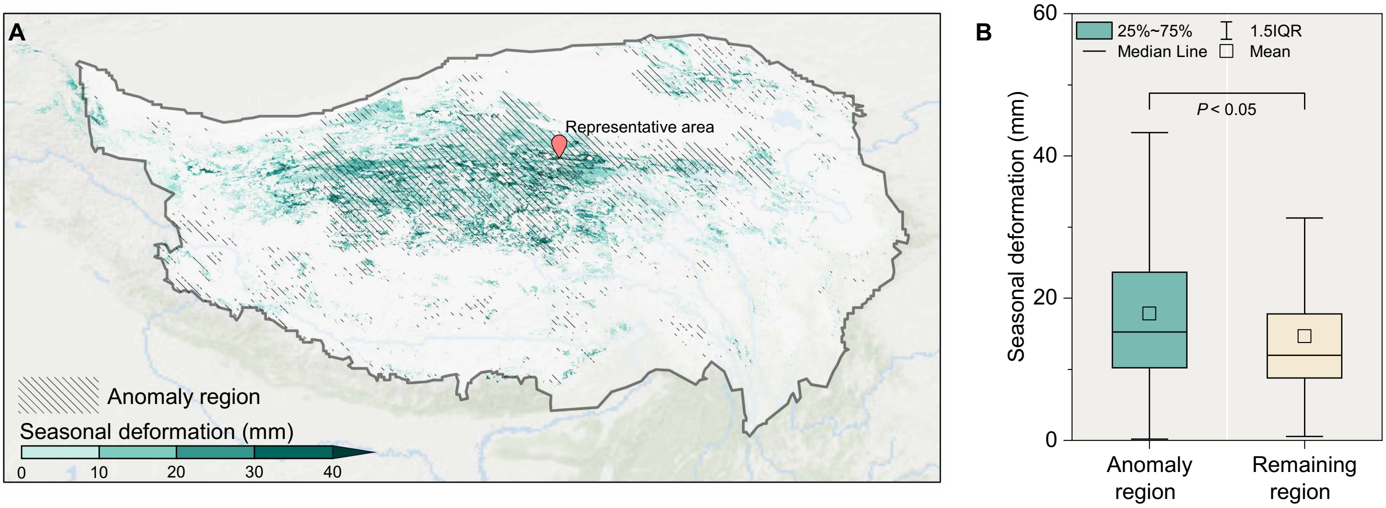

Fig. 4. Ground deformation associated with permafrost anomaly. (**A**) The annual average seasonal ground deformation amplitudes in the vertical direction of the plateau's permafrost regions from December 2014 to October 2022. (**B**) The boxplots of the distribution of seasonal deformation amplitudes in anomaly regions and the remaining permafrost regions, with the difference being statistically significant ($P < 0.05$) according to *t* test.

By integrating simulations from a region with substantial FWC increase and pronounced ground deformation (Fig. 5A), we present potential linkages between anomalous ice at active layer bottom and ground deformation (Fig. 5B). During the dry and cold pre-2000 period, ice content was generally scarce in the active layer, and associated ground deformations were limited (Fig. 5, A and B, stage 1). As precipitation has increased since 2000, ice starts to accumulate and forms an ice-rich zone at the bottom of the active layer (Fig. 5, A and B, stage 2) (*29*, *32*). The amplified volumetric changes associated with the freeze-thaw process of the increased ice may potentially result in greater frost heave and vertical ground surface deformation (*30*, *41*). Because of the latent heat effects, the ice-rich zone also resists the downward movement of the thaw front in summer and tends to promote interannual stability at the active layer bottom (*42*). However, as the climate further warms after approximately 2013, a progressive thaw penetrated into this ice-rich zone and melted the ice content (Fig. 5, A and B, stage 3). This change suggests that the identified anomalous ice gain and associated amplified ground deformation are likely transient rather than persistent processes. Future climate warming and active layer deepening may progressively thaw the accumulated ice at active layer bottom, potentially leading to the disappearance of the permafrost anomaly and weakening of the associated seasonal ground deformation.

DISCUSSION

The anomalous ice gain at active layer bottom in the interior Tibetan Plateau resembles the Karakoram Glacier Anomaly observed in the same region. Over the past few decades, anomalous glacier mass gains or near-balanced mass budgets have been reported in the Karakoram region despite ongoing climate warming (*33*, *43*), paralleling the anomalous ground ice accumulation identified in this study. Modern explanations of the Karakoram Glacier Anomaly primarily attribute its occurrence to the increase in winter snowfall from enhanced westerly dominated precipitation, which contributes to the glacier mass accumulation (*43*). Although the linkage between the permafrost and glacier anomalies remains uncertain, their concurrent ice mass gains indicate a novel and unique cryospheric response to the region's distinctive climatic conditions. The interplay between strengthening westerlies and weakening monsoons is suggested to have led to increased precipitation (*44*), thereby contributing to a positive regional ice budget encompassing glaciers, snow, and ground ice. Coordinated observations and investigations of these coevolving cryospheric components are essential for elucidating the coupled evolution of the cryosphere and its cascading impacts under climate change, which requires joint efforts across multiple scientific communities.

Such anomalous ice gain at active layer bottom is also likely prevalent across global permafrost regions. Its occurrence is primarily controlled by the increase in precipitation and persistently cold ground temperatures below the freezing point. Despite global warming, ground temperatures in most of the permafrost regions remain below 0°C (*2*, *5*), while rising precipitation has also been widely reported across typical permafrost areas such as Alaska, Siberia, and high mountain regions in Europe (*45*–*47*). The additional soil moisture supplied by enhanced precipitation can refreeze at the bottom of the active layer, leading to anomalous ice accumulation in these regions. Therefore, the permafrost anomaly and the associated ground destabilization identified on the Tibetan Plateau may occur widely across the Northern Hemisphere's permafrost regions.

Nevertheless, permafrost anomaly represents a temporary ice accumulation process rather than a sustained formation of ground ice. Although anomalous ice accumulation currently occurs widely on the Tibetan Plateau, the continued climate warming will progressively raise ground temperatures, eventually surpassing the freezing point and no longer supporting ice accumulation (*17*). The subsequent thaw of the anomalously accumulated ice has already been observed in the relatively warmer regions of the central plateau (Fig. 5A). Temperature-based future projections under various shared socioeconomic pathways suggest that while most present-day permafrost on the plateau is likely to persist until 2050, 44 to 71% may degrade by 2100 (*48*). A transition from anomalous ground ice accumulation to loss is expected in the future, further complicating permafrost dynamics.

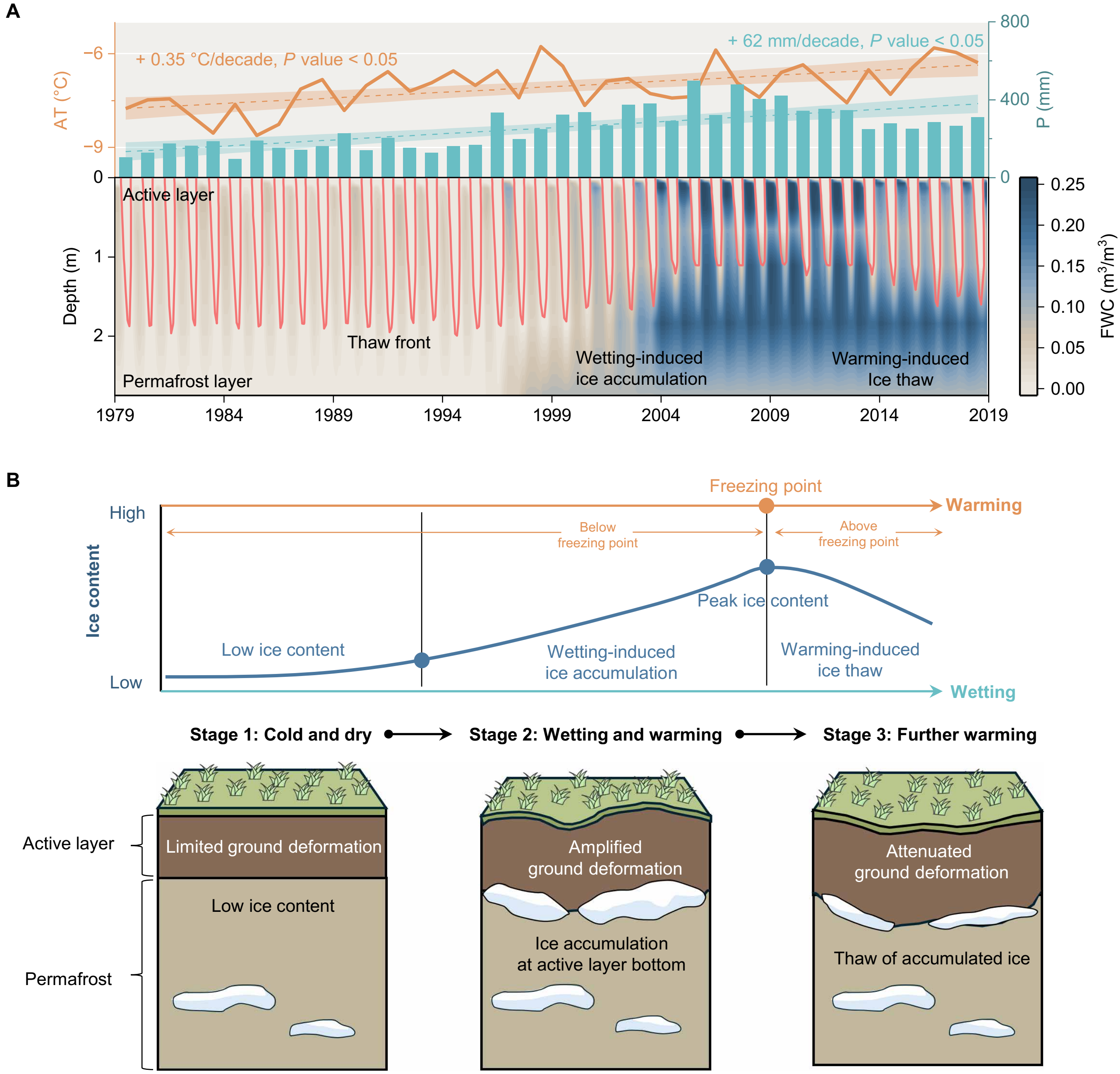

Fig. 5. Permafrost anomaly facilitates ground deformation and thermokarst development. (**A**) The simulated FWC changes and thaw front dynamics within soil profiles from 1979 to 2018 at the representative area with massive thaw slumps (marked in Fig. 4A), along with the associated air temperature and precipitation variations. (**B**) Conceptual framework illustrating the active layer ice content dynamics and the associated ground deformation under climate change.

Anomalous ice increase at active layer bottom also exerts impacts on regional landscape stability and has associated environmental and socioeconomic consequences. Active layer bottom acts as a transient layer at the interface between the seasonally frozen active layer and underlying long-term permafrost layer. The stability of near-surface permafrost is highly related to the dynamics of ice within the active layer bottom (*29*, *42*). As ice increases, the amplified ground deformation and the related landscape instability may promote the loss of sediment, solutes, and organic materials from the active layer (*40*, *49*). Infrastructure (i.e., buildings, roads, and bridges) and irrigation systems also face growing threats from associated ground deformation, leading to heightened demands for maintenance and replacement (*12*, *50*). In particular, the Tibetan Plateau serves as Asia's most important "water tower," holding the world's largest alpine river systems and providing freshwater to approximately two billion people downstream (*4*). Permafrost anomaly occurring near water systems can enhance thaw erosion processes and release substantial sediment (*51*, *52*), degrading the freshwater ecosystem and reshaping river morphology (*40*, *53*).

Understanding the role of precipitation in regulating permafrost dynamics is increasingly recognized as urgent (*54*). However, previous research has predominantly focused on atmospheric warming as the primary driver of permafrost degradation, while the impacts of precipitation changes on permafrost thermal-hydrological processes and near-surface ice content remain insufficiently quantified. This study reveals the previously unrecognized ice gain at active layer bottom driven by rapid precipitation increase in the Tibetan Plateau's permafrost regions, providing new insights into permafrost-climate interactions. The impacts of this anomalous ice gain on the stability of underlying permafrost and broader environmental and socioeconomic consequences remain open and important questions that warrant further investigation. We therefore recommend that future research should: (i) establish comprehensive monitoring networks to improve permafrost assessments, with particular attention to precipitation-induced ground ice dynamics; (ii) improve model representations of coupled thermal-hydrological processes and incorporate mechanisms governing excess ground ice formation and evolution; and (iii) prioritize the design and implementation of infrastructure that explicitly addresses landscape instability associated with anomalous ice gain within active layer.

MATERIALS AND METHODS

Permafrost and ground ice observations

We compiled field observations of permafrost hydrological and thermal characteristics from five long-term monitoring sites (*55*) and 369 boreholes across the permafrost regions of the Tibetan Plateau (Fig. 1A). The long-term monitoring sites are equipped with automated instruments that continuously record ST and liquid water content at multiple depths on a daily scale. Detailed information about these sites, including their locations, altitudes, observation depths, and monitoring periods, is presented in table S3. The boreholes provide observational data on ground ice content from near surface to depths of 20 m. Of the 369 boreholes, 223 are measured by the Qinghai-Tibet Plateau permafrost monitoring network established by the Cryosphere Research Station, Chinese Academy of Sciences (*23*) (table S1), and the remaining 146 are collected from published literature (table S2). The drilled soil samples from the boreholes were sealed and brought to the laboratory for ground ice content measurement. A dry-weight gravimetric method was used, wherein the ground ice content is quantified as the ratio of the mass of water lost during oven-drying (representing the original ice mass) to the dry mass of the sample. This gravimetric ice content was then converted to volumetric ice content using a transfer function (*27*).

Simulation of hydro-thermal variations of permafrost on the Tibetan Plateau

By integrating the Simultaneous Heat and Water (SHAW) model (*56*), a heat-and-water-coupled model, with high-quality forcing data, we established a modeling framework (*57*) to simulate the dynamics of ice with near-surface permafrost (0 to 3.2 m) on the Tibetan Plateau from 1979 to 2018 (fig. S1). The SHAW model is particularly well-suited for permafrost simulation due to its comprehensive representation of the complex heat and water exchange processes of frozen ground and their interactions within climate change, vegetation dynamics, and topography properties (*58*, *59*). Numerous studies have proven the robust performance of the SHAW model in permafrost environments (*59*–*62*). Specifically, the SHAW model incorporates multiple heat transfer mechanisms, including conductive heat transfer, convective heat transfer, latent heat exchange, and vapor migration, into its governing equation

$$\frac{\partial}{\partial z}\left(k_s\frac{\partial T}{\partial z}\right)-\rho_l c_l\frac{\partial\left(q_l T\right)}{\partial z}-L_v\left(\frac{\partial \rho_v}{\partial t}+\frac{\partial q_v}{\partial z}\right)=C_s\frac{\partial T}{\partial t}-\rho_i L_f\frac{\partial \theta_i}{\partial t} \quad (1)$$

where C_s is the effective volumetric heat capacity of the soil layer ($J\cdot m^{-3}\cdot°C^{-1}$), representing a lumped influence of minerals, liquid, ice, and vapor in the soil layer; T is the ST in this layer (°C); ρ_i, ρ_l, and ρ_v are the densities of ice, liquid water, and vapor ($kg\cdot m^{-3}$), respectively; L_f and L_v are the latent heats of fusion and vaporization ($kJ\cdot kg^{-1}$), respectively; θ_i is the FWC (representing pore ice) of the soil layer ($m^3\cdot m^{-3}$); q_l and q_v are the liquid water flux ($m\cdot s^{-1}$) and vapor flux ($kg\cdot m^{-2}\ s^{-1}$), respectively; k_s is the soil thermal conductivity ($W\cdot m^{-1}\cdot°C^{-1}$); c_l is the specific heat capacity of water ($J\cdot kg^{-1}\cdot°C^{-1}$); and t and z are the time step and the depth centered in the present layer. From left to right, the terms in the equation represent: heat conduction, heat convection due to liquid water migration, latent heat of evapotranspiration and vapor convection, temperature change, and latent heat of liquid-ice phase change. It should be noted that the FWC simulated by the SHAW model represents only pore-ice volume within frozen soil, while excluding the excess ice. Nevertheless, FWC can provide a reasonable proxy for changes in near-surface ground ice, which is particularly sensitive to recent climate warming and has critical implications for infrastructure stability, ecosystem processes, and carbon feedbacks.

We separate the entire Tibetan Plateau into 25,382 grids at a 0.1° spatial resolution (~10 km) and run the SHAW model to simulate the permafrost dynamics in each grid from 1979 to 2018. The inputs of the SHAW model include meteorological forcings, vegetation and soil parameters, and initial and lower boundary conditions. The required meteorological forcings consist of air temperature, wind speed, relative humidity, precipitation, and shortwave radiation. To drive the simulations, we use the China Meteorological Forcing Dataset (CMFD) (*63*), which provides high-quality meteorological data for the Tibetan Plateau from 1979 to 2018 at a 0.1° spatial resolution with a 3-hour temporal interval. The topographic controls (elevation, slope, and aspect) are generated from the 90-m resolution SRTM DEM and then aggregated to 0.1° resolution. The vegetation and soil texture types are extracted from the MODIS MCD12Q1 land use dataset and the Harmonized World Soil Database, respectively. The key vegetation and soil parameters are obtained from lookup tables provided by the Global Land Data Assimilation System (tables S4 and S5).

The vertical discretization of the soil column in the simulation consisted of 10 layers from 0- to 3.2-m depth, centered at 0.00, 0.02, 0.07, 0.13, 0.23, 0.39, 0.66, 1.1, 1.83, and 2.7 m. To initialize the SHAW model, the ST and moisture conditions of each layer on 1 January 1979 were obtained from the Noah-LSM simulations by Ji *et al.* (*64*), which have undergone a 500-year spin-up to minimize biases. To further reduce potential initialization biases, we apply an additional 40-year spin-up by repeatedly simulating the first four years (1979–1983). The lower boundary temperature and moisture conditions at 2.7-m depth are also sourced from Ji *et al.* (*64*). By integrating in situ ST observations and a random forest (RF) model, we reduce the uncertainties in Noah-LSM–simulated ST to improve its suitability as the lower boundary condition for SHAW (*57*). The RF predictors comprised 30-day averages of Noah-LSM–simulated STs at depths of 0.02, 0.39, and 2.7 m, while the target variables (the true temperature at 2.7-m depth) are obtained from observations at multiple permafrost monitoring sites across the Tibetan Plateau. The corrected lower boundary conditions were shown to substantially enhance the simulation accuracy of the SHAW model, particularly in the deeper soil layers (*57*).

Validation of the simulations

The model outputs include ST, SWC, and FWC at each soil depth, with a spatial resolution of 0.1° and a daily temporal interval from 1979 to 2018 across the Tibetan Plateau. The simulated ST and unfrozen moisture content (SWC-FWC) were validated against long-term in situ observations at multiple depths from representative permafrost monitoring sites (table S3). The Nash-Sutcliffe efficiencies for ST and unfrozen moisture content are generally greater than 0.7 and 0.4, respectively, with relatively low root mean square errors (figs. S2 and S3), indicating that the SHAW model reasonably captures variations in ST and water phase-change processes within frozen ground.

We further evaluate the simulated FWC using ground ice observations from borehole measurements. For consistency with the simulated soil column, borehole data are restricted to the upper 0 to 3 m using depth-weighted averaging and aggregated to 0.1° grid cells to match the model resolution and reduce local heterogeneity. In addition, simulated wintertime FWC is used instead of annual means to minimize the influence of seasonal freeze-thaw processes and better represent ground ice conditions. The wintertime FWC is then averaged by depth and aggregated to a multiannual scale to match borehole measurements. The comparison shows that simulated FWC reasonably captures the spatial distribution of near-surface ground ice across the study region (fig. S3M). Although FWC represents pore ice only, whereas borehole observations include both pore and excess ice, excess ice is relatively limited in the near-surface layer, suggesting that FWC can serve as a useful proxy for near-surface ground ice dynamics in response to climate change.

Scenario experiments

To disentangle the relative contributions of climate warming and wetting to the hydrological and thermal dynamics of permafrost, we conducted additional scenario experiments using the SHAW model under controlled climate forcing. The period 1979 to 1999 was used as the baseline climate condition, and two sensitivity scenarios were designed accordingly. In the No wetting scenario, precipitation after 2000 was replaced by the precipitation from the baseline period (1979–1999), while air temperature followed the post-2000 variations from the CMFD. In the No warming scenario, air temperature after 2000 was replaced by baseline temperature, while the precipitation variations from CMFD were retained. All other meteorological variables and model settings remained identical to those used in the simulation driven by the original CMFD forcing, which represents climate conditions with concurrent warming and wetting. By comparing simulations driven by these scenarios with the simulation driven by original CMFD forcing, the respective impacts of precipitation increase and atmospheric warming on FWC variations were quantified.

Ground deformation data

We derived multiyear ground deformation rates from satellite-based InSAR to analyze permafrost dynamics and ground deformation across the permafrost regions of the Tibetan Plateau. Deformation rates from 2015 to 2020 in permafrost regions are obtained from the multitemporal InSAR technique using the C-band Sentinel-1 SAR data (*65*). The time series of the ground deformation information includes both the multiyear long-term deformation velocity and seasonal deformation amplitude. Here, we disentangle the deformation time series using a combination of linear and trigonometric functions

$$D_t = D_{\text{multiyear}} + D_{\text{seasonal}} = at + \frac{b}{2}\sin\left[\frac{2\pi}{T}(t+\varphi)\right] + u \tag{2}$$

where a and $|b|$ refer to multiannual deformation velocity and seasonal deformation amplitude in the vertical direction, respectively; t is the time step, T is the cycle of seasonal deformation (set to 1 year), φ is an empirical parameter to fit the cyclic phase, and u is the noise. We use the least square methods to fit the parameters in the equation with the InSAR deformation time series at each grid. Therefore, the seasonal deformation amplitude in the vertical direction can be quantified. The original deformation data at 0.001° spatial resolution is aggregated to 0.1° to facilitate the direct comparison with the simulations from the SHAW model.

Permafrost data from CMIP6

We apply historical data (1975 to 2014) of FWC simulated by 10 models from CMIP6 to further evaluate the permafrost ice dynamics on the Tibetan Plateau. Model selection is based on the availability of monthly FWC data at 1° from the CMIP6 data server. The names of the 10 models are presented in fig. S7. Near-surface air temperature from the same models and at the same spatial-temporal resolution is also used to assess temperature changes. Monthly data were aggregated into annual averages, and change rates were calculated using linear regression. Subsequently, the covariations in FWC and temperature across the 10 models are quantified and used to further evaluate the ground ice changes on the Tibetan Plateau.

Supplementary Materials

This PDF file includes:
Figs. S1 to S9
Tables S1 to S5
References

REFERENCES

1. J. Obu, How much of the Earth's surface is underlain by permafrost? *Case Rep. Med.* **126**, e2021JF006123 (2021).
2. B. K. Biskaborn, S. L. Smith, J. Noetzli, H. Matthes, G. Vieira, D. A. Streletskiy, P. Schoeneich, V. E. Romanovsky, A. G. Lewkowicz, A. Abramov, M. Allard, J. Boike, W. L. Cable, H. H. Christiansen, R. Delaloye, B. Diekmann, D. Drozdov, B. Etzelmüller, G. Grosse, M. Guglielmin, T. Ingeman-Nielsen, K. Isaksen, M. Ishikawa, M. Johansson, H. Johannsson, A. Joo, D. Kaverin, A. Kholodov, P. Konstantinov, T. Kröger, C. Lambiel, J.-P. Lanckman, D. Luo, G. Malkova, I. Meiklejohn, N. Moskalenko, M. Oliva, M. Phillips, M. Ramos, A. B. K. Sannel, D. Sergeev, C. Seybold, P. Skryabin, A. Vasiliev, Q. Wu, K. Yoshikawa, M. Zheleznyak, H. Lantuit, Permafrost is warming at a global scale. *Nat. Commun.* **10**, 264 (2019).
3. J. Nitzbon, T. Schneider von Deimling, M. Aliyeva, S. E. Chadburn, G. Grosse, S. Laboor, H. Lee, G. Lohmann, N. J. Steinert, S. M. Stuenzi, M. Werner, S. Westermann, M. Langer, No respite from permafrost-thaw impacts in the absence of a global tipping point. *Nat. Clim. Change* **14**, 573–585 (2024).
4. T. Yao, T. Bolch, D. Chen, J. Gao, W. Immerzeel, S. Piao, F. Su, L. Thompson, Y. Wada, L. Wang, T. Wang, G. Wu, B. Xu, W. Yang, G. Zhang, P. Zhao, The imbalance of the Asian water tower. *Nat. Rev. Earth Environ.* **3**, 618–632 (2022).
5. X. Wang, Y. Ran, G. Pang, D. Chen, B. Su, R. Chen, X. Li, H. W. Chen, M. Yang, X. Gou, M. T. Jorgenson, J. Aalto, R. Li, X. Peng, T. Wu, G. D. Clow, G. Wan, X. Wu, D. Luo, Contrasting characteristics, changes, and linkages of permafrost between the Arctic and the Third Pole. *Earth Sci. Rev.* **230**, 104042 (2022).

6. N. Pepin, R. S. Bradley, H. F. Diaz, M. Baraer, E. B. Caceres, N. Forsythe, H. Fowler, G. Greenwood, M. Z. Hashmi, X. D. Liu, J. R. Miller, L. Ning, A. Ohmura, E. Palazzi, I. Rangwala, W. Schöner, I. Severskiy, M. Shahgedanova, M. B. Wang, S. N. Williamson, D. Q. Yang, Mountain Research Initiative EDW Working Group, Elevation-dependent warming in mountain regions of the world. *Nat. Clim. Change* **5**, 424–430 (2015).
7. E. A. G. Schuur, A. D. McGuire, C. Schädel, G. Grosse, J. W. Harden, D. J. Hayes, G. Hugelius, C. D. Koven, P. Kuhry, D. M. Lawrence, S. M. Natali, D. Olefeldt, V. E. Romanovsky, K. Schaefer, M. R. Turetsky, C. C. Treat, J. E. Vonk, Climate change and the permafrost carbon feedback. *Nature* **520**, 171–179 (2015).
8. M. M. P. D. Heijmans, R. Í. Magnússon, M. J. Lara, G. V. Frost, I. H. Myers-Smith, J. van Huissteden, M. T. Jorgenson, A. N. Fedorov, H. E. Epstein, D. M. Lawrence, J. Limpens, Tundra vegetation change and impacts on permafrost. *Nat. Rev. Earth Environ.* **3**, 68–84 (2022).
9. J. Hjort, D. Streletskiy, G. Doré, Q. Wu, K. Bjella, M. Luoto, Impacts of permafrost degradation on infrastructure. *Nat. Rev. Earth Environ.* **3**, 24–38 (2022).
10. A. K. Liljedahl, J. Boike, R. P. Daanen, A. N. Fedorov, G. V. Frost, G. Grosse, L. D. Hinzman, Y. Iijma, J. C. Jorgenson, N. Matveyeva, M. Necsoiu, M. K. Raynolds, V. E. Romanovsky, J. Schulla, K. D. Tape, D. A. Walker, C. J. Wilson, H. Yabuki, D. Zona, Pan-Arctic ice-wedge degradation in warming permafrost and its influence on tundra hydrology. *Nat. Geosci.* **9**, 312–318 (2016).
11. L. Wang, L. Zhao, H. Zhou, S. Liu, G. Hu, Z. Li, C. Wang, J. Zhao, Evidence of ground ice melting detected by InSAR and in situ monitoring over permafrost terrain on the Qinghai-Xizang (Tibet) Plateau. *Permafr. Periglac. Process.* **34**, 52–67 (2023).
12. Y. Ran, G. Cheng, Y. Dong, J. Hjort, A. L. Lovecraft, S. Kang, M. Tan, X. Li, Permafrost degradation increases risk and large future costs of infrastructure on the Third Pole. *Commun. Earth Environ.* **3**, 238 (2022).
13. J. C. Stroeve, D. Notz, J. Dawson, E. A. G. Schuur, D. Dahl-Jensen, C. Giesse, Disappearing landscapes: The Arctic at +2.7°C global warming. *Science* **387**, 616–621 (2025).
14. C. Mu, P. Lei, M. Mu, C. Zhang, Z. Zhou, J. Song, Y. Jia, C. Fan, X. Peng, G. Zhang, Y. Yang, L. Wang, D. Li, C. Song, G. Wang, Z. Zhang, Methane emissions from thermokarst lakes must emphasize the ice-melting impact on the Tibetan Plateau. *Nat. Commun.* **16**, 2404 (2025).
15. G. Wang, Y. Peng, L. Chen, B. W. Abbott, P. Ciais, L. Kang, Y. Liu, Q. Li, J. Peñuelas, S. Qin, P. Smith, Y. Song, J. Strauss, J. Wang, B. Wei, J. Yu, D. Zhang, Y. Yang, Enhanced response of soil respiration to experimental warming upon thermokarst formation. *Nat. Geosci.* **17**, 532–538 (2024).
16. M. R. Turetsky, B. W. Abbott, M. C. Jones, K. W. Anthony, D. Olefeldt, E. A. G. Schuur, G. Grosse, P. Kuhry, G. Hugelius, C. Koven, D. M. Lawrence, C. Gibson, A. B. K. Sannel, A. D. McGuire, Carbon release through abrupt permafrost thaw. *Nat. Geosci.* **13**, 138–143 (2020).
17. T. Wang, D. Yang, Y. Yang, G. Zheng, H. Jin, X. Li, T. Yao, G. Cheng, Unsustainable water supply from thawing permafrost on the Tibetan Plateau in a changing climate. *Sci. Bull.* **68**, 1105–1108 (2023).
18. F. Xu, G. Zhang, R. I. Woolway, K. Yang, Y. Wada, J. Wang, J.-F. Crétaux, Widespread societal and ecological impacts from projected Tibetan Plateau lake expansion. *Nat. Geosci.* **17**, 516–523 (2024).
19. L. Wang, L. Zhao, H. Zhou, S. Liu, G. Liu, D. Zou, E. Du, G. Hu, C. Wang, Quantification of water released by thawing permafrost in the source region of the Yangtze River on the Tibetan Plateau by InSAR monitoring. *Water Resour. Res.* **59**, e2023WR034451 (2023).
20. D. Li, X. Lu, I. Overeem, D. E. Walling, J. Syvitski, A. J. Kettner, B. Bookhagen, Y. Zhou, T. Zhang, Exceptional increases in fluvial sediment fluxes in a warmer and wetter High Mountain Asia. *Science* **374**, 599–603 (2021).
21. T. Zhang, D. Li, A. E. East, A. J. Kettner, J. Best, J. Ni, X. Lu, Shifted sediment-transport regimes by climate change and amplified hydrological variability in cryosphere-fed rivers. *Sci. Adv.* **9**, eadi5019 (2023).
22. D. Li, X. Lu, D. E. Walling, T. Zhang, J. F. Steiner, R. J. Wasson, S. Harrison, S. Nepal, Y. Nie, W. W. Immerzeel, D. H. Shugar, M. Koppes, S. Lane, Z. Zeng, X. Sun, A. Yegorov, T. Bolch, High Mountain Asia hydropower systems threatened by climate-driven landscape instability. *Nat. Geosci.* **15**, 520–530 (2022).
23. L. Zhao, Y. Ding, G. Liu, S. Wang, H. Jin, Estimates of the reserves of ground ice in permafrost regions on the Tibetan Plateau. *J. Glaciol. Geocryol.* **32**, 1–9 (2010).
24. F. Chen, L. Ding, S. Piao, T. Zhou, B. Xu, T. Yao, X. Li, The Tibetan Plateau as the engine for Asian environmental change: The Tibetan Plateau Earth system research into a new era. *Sci. Bull.* **66**, 1263–1266 (2021).
25. N. J. Steinert, M. V. Debolskiy, E. J. Burke, F. García-Pereira, H. Lee, Evaluating permafrost definitions for global permafrost area estimates in CMIP6 climate models. *Environ. Res. Lett.* **19**, 014033 (2023).
26. L. Cai, H. Lee, K. S. Aas, S. Westermann, Projecting circum-Arctic excess-ground-ice melt with a sub-grid representation in the Community Land Model. *Cryosphere* **14**, 4611–4626 (2020).
27. D. Zou, Q. Pang, L. Zhao, L. Wang, G. Hu, E. Du, G. Liu, S. Liu, Y. Liu, Estimation of Permafrost Ground Ice to 10 m Depth on the Qinghai-Tibet Plateau. *Permafr. Periglac. Process.* **35**, 423–434 (2024).
28. R. Í. Magnússon, A. Hamm, S. V. Karsanaev, J. Limpens, D. Kleijn, A. Frampton, T. C. Maximov, M. M. P. D. Heijmans, Extremely wet summer events enhance permafrost thaw for multiple years in Siberian tundra. *Nat. Commun.* **13**, 1556 (2022).
29. D. A. Streletskiy, A. Maslakov, G. Grosse, N. I. Shiklomanov, L. Farquharson, S. Zwieback, G. Iwahana, A. Bartsch, L. Liu, T. Strozzi, H. Lee, M. V. Debolskiy, Thawing permafrost is subsiding in the Northern Hemisphere—Review and perspectives. *Environ. Res. Lett.* **20**, 013006 (2025).
30. Z. Zhang, Q. Wang, Q. Jin, M. Wang, Exploring ground ice dynamics in central Qinghai–Tibet Plateau permafrost region using SAR Interferometry, Landsat, and ICESat-2 Data. *J. Climate* **38**, 2719–2737 (2025).
31. U. Mishra, G. Hugelius, E. Shelef, Y. Yang, J. Strauss, A. Lupachev, J. W. Harden, J. D. Jastrow, C.-L. Ping, W. J. Riley, E. A. G. Schuur, R. Matamala, M. Siewert, L. E. Nave, C. D. Koven, M. Fuchs, J. Palmtag, P. Kuhry, C. C. Treat, S. Zubrzycki, F. M. Hoffman, B. Elberling, P. Camill, A. Veremeeva, A. Orr, Spatial heterogeneity and environmental predictors of permafrost region soil organic carbon stocks. *Sci. Adv.* **7**, eaaz5236 (2021).
32. Z. Fu, Q. Wu, W. Zhang, H. He, L. Wang, Water migration and segregated ice formation in frozen ground: Current advances and future perspectives. *Front. Earth Sci.* **10**, 826961 (2022).
33. T. Yao, L. Thompson, W. Yang, W. Yu, Y. Gao, X. Guo, X. Yang, K. Duan, H. Zhao, B. Xu, J. Pu, A. Lu, Y. Xiang, D. B. Kattel, D. Joswiak, Different glacier status with atmospheric circulations in Tibetan Plateau and surroundings. *Nat. Clim. Change* **2**, 663–667 (2012).
34. J. Wang, C. Wang, Y. Yang, Y. Peng, J. Gao, C. Shi, Y. Chen, P. Ciwang, Y. Dong, S. Ha, X. Jiang, More rapid reduction of spring snow cover on the Western Tibetan Plateau by emergent constraint. *Geophys. Res. Lett.* **53**, e2025GL119124 (2026).
35. G. Hu, Z. Sun, L. Zhao, D. Chen, D. Zou, C.-L. Ping, W. Zhang, Y. Xiao, G. Liu, R. Li, X. Wu, Y. Wu, G. Cheng, The crucial role of ground ice in slowing permafrost degradation. *Sci. Bull.* **71**, 1641–1644 (2026).
36. B. Groenke, M. Langer, J. Nitzbon, S. Westermann, G. Gallego, J. Boike, Investigating the thermal state of permafrost with Bayesian inverse modeling of heat transfer. *Cryosphere* **17**, 3505–3533 (2023).
37. Q. Li, X. Peng, O. W. Frauenfeld, Z. Wu, Y. Wang, C. Mu, Extreme rainfall reshapes permafrost thermal regimes across the Northern Hemisphere. *Nat. Commun.* **17**, 3204 (2026).
38. J. Chen, T. Wu, D. Zou, L. Liu, X. Wu, W. Gong, X. Zhu, R. Li, J. Hao, G. Hu, Q. Pang, J. Zhang, S. Yang, Magnitudes and patterns of large-scale permafrost ground deformation revealed by Sentinel-1 InSAR on the central Qinghai-Tibet Plateau. *Remote Sens. Environ.* **268**, 112778 (2022).
39. T. Chang, Y. Yi, H. Jiang, R. Li, P. Lu, L. Liu, L. Wang, L. Zhao, S. Zwieback, J. Zhao, Unraveling the non-linear relationship between seasonal deformation and permafrost active layer thickness. *Npj Clim. Atmos. Sci.* **7**, 308 (2024).
40. T. Zhang, D. Li, A. E. East, D. E. Walling, S. Lane, I. Overeem, A. A. Beylich, M. Koppes, X. Lu, Warming-driven erosion and sediment transport in cold regions. *Nat. Rev. Earth Environ.* **3**, 832–851 (2022).
41. S. Liu, L. Zhao, L. Wang, L. Liu, D. Zou, G. Hu, Z. Sun, Y. Zhang, W. Chen, X. Wang, M. Wang, H. Zhou, Y. Qiao, Ground surface deformation in permafrost region on the Qinghai-Tibet Plateau: A review. *Earth Sci. Rev.* **265**, 105109 (2025).
42. Y. Shur, K. M. Hinkel, F. E. Nelson, The transient layer: Implications for geocryology and climate-change science. *Permafr. Periglac. Process.* **16**, 5–17 (2005).
43. D. Farinotti, W. W. Immerzeel, R. J. de Kok, D. J. Quincey, A. Dehecq, Manifestations and mechanisms of the Karakoram glacier Anomaly. *Nat. Geosci.* **13**, 8–16 (2020).
44. J. Jiang, T. Zhou, Y. Qian, C. Li, F. Song, H. Li, X. Chen, W. Zhang, Z. Chen, Precipitation regime changes in High Mountain Asia driven by cleaner air. *Nature* **623**, 544–549 (2023).
45. R. Bintanja, O. Andry, Towards a rain-dominated Arctic. *Nat. Clim. Change* **7**, 263–267 (2017).
46. M. R. McCrystall, J. Stroeve, M. Serreze, B. C. Forbes, J. A. Screen, New climate models reveal faster and larger increases in Arctic precipitation than previously projected. *Nat. Commun.* **12**, 6765 (2021).
47. J. Noetzli, K. Isaksen, J. Barnett, H. H. Christiansen, R. Delaloye, B. Etzelmüller, D. Farinotti, T. Gallemann, M. Guglielmin, C. Hauck, C. Hilbich, M. Hoelzle, C. Lambiel, F. Magnin, M. Oliva, L. Paro, P. Pogliotti, C. Riedl, P. Schoeneich, M. Valt, A. Vieli, M. Phillips, Enhanced warming of European mountain permafrost in the early 21st century. *Nat. Commun.* **15**, 10508 (2024).
48. G. Zhang, Z. Nan, N. Hu, Z. Yin, L. Zhao, G. Cheng, C. Mu, Qinghai-Tibet Plateau permafrost at risk in the late 21st century. *Earth's Future* **10**, e2022EF002652 (2022).
49. D. Li, I. Overeem, A. J. Kettner, Y. Zhou, X. Lu, Air temperature regulates erodible landscape, water, and sediment fluxes in the permafrost-dominated catchment on the Tibetan Plateau. *Water Resour. Res.* **57**, e2020WR028193 (2021).
50. F. Niu, J. Luo, Distribution Data of Freezing-thawing Hazards in Qinghai Tibet Engineering Corridor (2019–2020), National Tibetan Plateau / Third Pole Environment Data Center (2022); https://doi.org/https://doi.org/10.11888/RemoteSen.tpdc.272881.
51. A. G. Lewkowicz, R. G. Way, Extremes of summer climate trigger thousands of thermokarst landslides in a High Arctic environment. *Nat. Commun.* **10**, 1329 (2019).
52. S. V. Kokelj, J. Kokoszka, J. van der Sluijs, A. C. A. Rudy, J. Tunnicliffe, S. Shakil, S. E. Tank, S. Zolkos, Thaw-driven mass wasting couples slopes with downstream systems, and effects propagate through Arctic drainage networks. *Cryosphere* **15**, 3059–3081 (2021).

53. A. Sha, D. Li, D. Walling, Y. Zhao, S. Tian, D. Chen, S. Deng, J. Xia, J. Best, Accelerated river meander migration on the Tibetan Plateau caused by permafrost thaw. *Geophys. Res. Lett.* **52**, e2024GL111536 (2025).
54. Z. Fu, Q. Wu, A. Chen, L. Wang, G. Jiang, S. Gao, H. Yun, J. Chen, Non-temperature environmental drivers modulate warming-induced 21st-century permafrost degradation on the Tibetan Plateau. *Nat. Commun.* **16**, 7556 (2025).
55. L. Zhao, D. Zou, G. Hu, T. Wu, E. Du, G. Liu, Y. Xiao, R. Li, Q. Pang, Y. Qiao, X. Wu, Z. Sun, Z. Xing, Y. Sheng, Y. Zhao, J. Shi, C. Xie, L. Wang, C. Wang, G. Cheng, A synthesis dataset of permafrost thermal state for the Qinghai–Tibet (Xizang) Plateau, China. *Earth Syst. Sci. Data* **13**, 4207–4218 (2021).
56. G. N. Flerchinger, K. E. Saxton, Simultaneous heat and water model of a freezing snow-residue-soil system I. Theory and development. *Trans. ASAE* **32**, 565–571 (1989).
57. Y. Zhao, Z. Nan, H. Ji, Y. Chen, M. Ou, D. Li, A hybrid modeling approach for improved simulation of thermal-hydrological dynamics in active layer on the Qinghai-Tibet Plateau. *Water Resour. Res.* **61**, e2025WR040288 (2025).
58. G. N. Flerchinger, *The Simultaneous Heat and Water* (*SHAW*) *Model: Technical Documentation* (Northwest Watershed Research Center USDA Agricultural Research Service, Boise, Idaho, 2000).
59. Y. Zhao, Z. Nan, Z. Cao, H. Ji, J. Hu, Evaluation of parameterization schemes for matric potential in frozen soil in land surface models: A modeling perspective. *Water Resour. Res.* **59**, e2023WR034644 (2023).
60. L. Cui, Y. Zhu, T. Zhao, M. Ye, J. Yang, J. Wu, Evaluation of upward flow of groundwater to freezing soils and rational per-freezing water table depth in agricultural areas. *J. Hydrol.* **585**, 124825 (2020).
61. N. Li, L. Wang, D. Chen, Vegetation greening amplifies shallow soil temperature warming on the Tibetan Plateau. *Npj Clim. Atmos. Sci.* **7**, 118 (2024).
62. Y. Zhao, Z. Nan, H. Ji, L. Zhao, Convective heat transfer of spring meltwater accelerates active layer phase change in Tibet permafrost areas. *Cryosphere* **16**, 825–849 (2022).
63. J. He, K. Yang, W. Tang, H. Lu, J. Qin, Y. Chen, X. Li, The first high-resolution meteorological forcing dataset for land process studies over China. *Sci. Data* **7**, 25 (2020).
64. H. Ji, Z. Nan, J. Hu, Y. Zhao, Y. Zhang, On the spin-up strategy for spatial modeling of permafrost dynamics: A case study on the Qinghai-Tibet Plateau. *J. Adv. Model. Earth Syst.* **14**, e2021MS002750 (2022).
65. X. Hu, R. Bürgmann, X. Xu, E. Fielding, Z. Liu, Machine-learning characterization of tectonic, hydrological and anthropogenic sources of active ground deformation in California. *J. Geophys. Res. Solid Earth* **126**, e2021JB022373 (2021).
66. F. Wu, Q. You, J. Zhang, Z. Cai, Y. Yu, S. Kang, G. W. K. Moore, P. Zhai, Understanding of CMIP6 surface temperature cold bias over the westerly and monsoon regions of the Tibetan Plateau. *Climate Dynam.* **62**, 4133–4153 (2024).
67. Y. Yang, X. Guo, Q. Wu, H. Jin, F. Liu, Formation processes of shallow ground ice in permafrost in the Northeastern Qinghai-Tibet Plateau: A stable isotope perspective. *Sci. Total Environ.* **863**, 160967 (2023).
68. F. Niu, C. Jiao, J. Luo, J. He, P. He, Three-dimensional numerical modeling of ground ice ablation in a retrogressive thaw slump and its hydrological ecosystem response on the Qinghai-Tibet Plateau, China. *Int. J. Disaster Risk Sci.* **14**, 566–585 (2023).
69. X. Fan, Y. Wang, F. Niu, W. Li, X. Wu, Z. Ding, W. Pang, Z. Lin, Environmental characteristics of high ice-content permafrost on the Qinghai–Tibetan Plateau. *Remote Sens.* **15**, 4496 (2023).
70. G. Jiang, S. Gao, A. G. Lewkowicz, H. Zhao, S. Pang, Q. Wu, Development of a rapid active layer detachment slide in the Fenghuoshan Mountains, Qinghai–Tibet Plateau. *Permafr. Periglac. Process.* **33**, 298–309 (2022).
71. X. Fan, Z. Lin, Z. Gao, X. Meng, F. Niu, J. Luo, G. Yin, F. Zhou, A. Lan, Cryostructures and ground ice content in ice-rich permafrost area of the Qinghai-Tibet Plateau with Computed Tomography Scanning. *J. Mt. Sci.* **18**, 1208–1221 (2021).
72. S. Wang, Y. Sheng, J. Li, J. Wu, W. Cao, S. Ma, An estimation of ground ice volumes in permafrost layers in Northeastern Qinghai-Tibet Plateau, China. *Chin. Geogr. Sci.* **28**, 61–73 (2018).
73. F. Yu, J. Qi, X. Yao, Y. Liu, In-situ monitoring of settlement at different layers under embankments in permafrost regions on the Qinghai–Tibet Plateau. *Eng. Geol.* **160**, 44–53 (2013).
74. Y. You, Q. Yu, X. Pan, X. Wang, L. Guo, Application of electrical resistivity tomography in investigating depth of permafrost base and permafrost structure in Tibetan Plateau. *Cold Reg. Sci. Technol.* **87**, 19–26 (2013).
75. G. Yin, F. Niu, Z. Lin, J. Luo, M. Liu, Effects of local factors and climate on permafrost conditions and distribution in Beiluhe basin, Qinghai-Tibet Plateau, China. *Sci. Total Environ.* **581-582**, 472–485 (2017).

Acknowledgments: We thank R. Magnússon from Wageningen University & Research, G. Grosse and I. Nitze from Alfred Wegener Institute Helmholtz Centre for Polar and Marine Research, and V. Romanovsky from University of Alaska Fairbanks for the earlier discussion. **Funding:** This work was supported by the Fundamental and Interdisciplinary Disciplines Breakthrough Plan of the Ministry of Education of China (JYB2025XDXM910 to D.L.), the National Natural Science Foundation of China (52479055 and W2521152 to D.L., 42501152 to Y.Z., and 42525105 to Y.R.), China Postdoctoral Science Foundation (2025M770375 to Y.Z.), and the Innovation Platform Construction Project of Qinghai Province (2025-ZJ-J09 to D.L.). **Author contributions:** Conceptualization: Y.Z., D.L., and Z.N. Methodology: Y.Z., D.L., and Y.S. Software: Y.Z., D.L., and S.T. Validation: Y.Z. and D.L. Formal analysis: Y.Z., D.L., and Y.Li. Investigation: Y.Z., D.L., J.N., X.H., R.D., and Y.Luo. Data curation: Y.Z., D.L., and X.H. Writing—original draft: Y.Z. and D.L. Writing—review and editing: Y.Z., D.L., J.N., Z.N., X.H., and Y.R. Visualization: Y.Z., D.L., and S.T. Supervision: Y.Z. and D.L. Project administration: D.L. Resources: Y.Z., D.L., X.H., and Y.R. Funding acquisition: D.L. and Y.R. **Competing interests:** The authors declare that they have no competing interests. **Data, code, and materials availability:** All data generated or analyzed during this study and needed to evaluate or reproduce the results are included in the published article, the Supplementary Materials, and/or the following repositories. The source codes of the SHAW model are available on the USDA Agricultural Research Service website (https://ars.usda.gov/pacific-west-area/boise-id/northwest-watershed-research-center/docs/shaw-model/, accessed 3 April 2026). An improved version of the SHAW model applied in this study is available at https://doi.org/10.6084/m9.figshare.20884237.v2 (accessed 3 April 2026). The meteorological forcing data from CMFD are available at the National Tibetan Plateau Data Center (https://doi.org/10.11888/AtmosphericPhysics.tpe.249369.file, accessed 3 April 2026). The simulation data conducted by this study and the codes for analysis are available at https://doi.org/10.6084/m9.figshare.29634872. This study did not generate new materials.

Submitted 16 October 2025
Accepted 12 June 2026
Published 23 July 2026
10.1126/sciadv.aed1105

Science Advances

Westerly induced precipitation increase drives near-surface ground ice gain on the Tibetan Plateau despite warming

Yi Zhao, Dongfeng Li, Jan Nitzbon, Zhuotong Nan, Yuqi Song, Xie Hu, Youhua Ran, Shang Tian, Rui Deng, Yingzhong Luo, and Yiyi Li

Sci. Adv. **12** (30), eaed1105. DOI: 10.1126/sciadv.aed1105

Science Advances (ISSN 2375-2548) is published by the American Association for the Advancement of Science. 1200 New York Avenue NW, Washington, DC 20005. The title *Science Advances* is a registered trademark of AAAS.